Measurement of Biomass Moisture Content Distribution in a Fluidised Bed Dryer Through Electrostatic Sensing and Digital Imaging

Bojian Qi[1], Yong Yan[2,*], Wenbiao Zhang[1], Xueyao Wang[1]

1. School of Control and Computer Engineering, North China Electric Power University, Beijing 102206, China
2. School of Engineering and Digital Arts, University of Kent, Canterbury, Kent CT2 7NT, UK

(* Corresponding author: y.yan@kent.ac.uk)

Abstract

Accurate moisture content distribution measurement of biomass in a fluidised bed dryer is desirable to explore the complex drying characteristics, continuously monitor the operation and maximise the efficiency of the drying process. In this paper, electrostatic sensing and digital imaging techniques are combined to measure the moisture content distribution of biomass in a laboratory-scale fluidised bed dryer. The proposed method determines the biomass velocity by the cross correlation of the electrostatic sensor signals and establishes a measurement model that relates the root mean square of the sensor signals, the biomass velocity and the moisture content. Experimental tests are conducted under different inlet air velocities and temperatures to assess the electrostatic measurement method and investigate the moisture content distribution. The results demonstrate that the proposed method is capable of measuring the moisture content with a relative error within ±15%. Moreover, an optical digital imaging unit is used to record the positions of bubbles and the biomass in the fluidised bed. The mass transfer at the interface between the air and the biomass is determined by fusing the information from the moisture content and bubble positions.

Keywords: *Fluidised bed dryer; moisture content distribution; biomass; electrostatic sensing; digital imaging; mass transfer*

Nomenclature

Symbols

a	Fitted coefficient in Eq. (6) (V^{-1})
b	Fitted coefficient in Eq. (6) (-)
C	Equivalent capacitance (F)
c	Fitted coefficient in Eq. (7) ($s\ m^{-1}\ V^{-1}$))
d	Fitted coefficient in Eq. (7) (-)
e	Fitted coefficient in Eq. (7) (V^{-1})
k_c	Charging coefficient (-)
L_{gk}	Axial distance between electrodes (m)
M	Moisture content (wt. %).

M_0 Initial moisture content (wt. %).

q Particle charge (C)

q_s Saturation charge (C)

$\overline{RMS}$ Average RMS value of the electrostatic signals (V)

S Equivalent particle area (m^2)

V Equivalent potential difference (V)

v_{gk} Particle correlation velocity (m/s)

x Abscissa of the particle position (m)

y Ordinate of the particle position (m)

z Distance between a charged particle and an electrode (m)

Greek letters

α Charge generation coefficient (-)

β Charge dissipation coefficient (-)

ε Permittivity of the medium (F/m)

τ_{gk} Time delay (s)

1. Introduction

Biomass is a renewable fuel used as a substitute of fossil fuels in electric power and heat generation industries [1]. Drying is essential for the pre-processing of raw biomass materials to quickly remove the moisture, prevent the fungal growth, extend the storage time and meet the moisture content requirements for biomass power plants. Currently, fluidised bed dryers are widely used for the biomass drying due to their advantages of high rate of moisture removal and high thermal efficiency [2, 3]. The efficiency of heat and mass transfer is enhanced by enabling solid materials to contact effectively with the drying air at the gas-solid interface. Therefore, the moisture content distribution at the interface between the biomass and air is far more useful than local or average moisture content in a bed section [4]. Moreover, there are channelling and hotspot formation in fluidised bed dryers, leading to high moisture variations and hence low product quality [5]. Therefore, a reliable and accurate measurement of the moisture content distribution is desirable for the continuous monitoring the biomass drying operation, the fundamental understanding of drying kinetics and the optimization of fluidised bed dryers.

Over the last few decades, a variety of methods have been developed for the measurement of the moisture content distribution, such as near-infrared (NIR) hyperspectral imaging [6, 7], magnetic resonance imaging (MRI) [8], computed tomography (CT) scanning [9] and electrical capacitance tomography (ECT) [10, 11]. Even these methods are capable of visualising the moisture content distribution, there are also some drawbacks. The feasibility of using NIR hyperspectral imaging for moisture analysis is mainly due to the high absorbance of the NIR radiation by water. He *et al*. [6] used laboratory NIR hyperspectral imaging systems to acquire the moisture content distribution of salmon fillets, which were placed on the loading platform and conveyed to the field of view of spectrograph to be scanned line by line. However, the greatest

disadvantage of NIR hyperspectral imaging technique is the high cost and the large amounts of data produced for single measurement, which leads to the NIR hyperspectral imaging is unsuitable to be a reliable and efficient real-time system for industrial applications [12]. Moisture distribution is capable of being analysed quantitatively by using moisture distribution profiles generated from nuclear magnetic resonance signal intensity profiles of the magnetic resonance images. Horigane *et al*. [8] measured the moisture distribution in grains by MRI during soaking, and visualized the pattern and speed of water penetration. However, MRI depends on the chemical composition of material species and the bore size of the magnet in the apparatus. What's more, some improvements, primarily in relation to image acquisition time and software, should be developed to fulfil the requirements of the manufacturing industries.

CT scanning is a method that uses X-ray radiation to determine density distribution and hence the moisture content distribution within a plane section of a body, but a careful shielding is necessary to avoid radiation hazards [9]. ECT is a method to measure the moisture content distribution based on the permittivity distribution of the wet medium which is obtained by calculating electrical capacitances of the medium [11]. However, this technique suffers from several drawbacks, including long scan time, relatively high construction cost and sensitive to reconstruction algorithms [2]. In view of these disadvantages, the application of ECT to industrial fluidised bed dryers is very limited. Therefore, a new non-intrusive method for the moisture content distribution measurement is desirable to overcome the above drawbacks.

Electrostatic sensing is a passive, low-cost and non-intrusive technique, however, as the charging characteristics are affected by many factors, its potential to measure the moisture content distribution in a fluidised bed need to be evaluated. It is well known that triboelectric charging is inevitable due to continuous particle-particle, particle-wall, and particle-air interactions in the fluidised bed [13]. Numerous experimental studies have been reported that the moisture content has a significant impact on the charge of bulk solids material [14, 15]. Choi *et al*. [14] quantified the conductivity of pharmaceutical powders at various moisture contents and correlated them with the charge dissipation when the moisture content increased. Taghavivand *et al*. [15] investigated the effects of drying kinetics on triboelectric charging behaviour of pharmaceutical granules in a fluidised bed dryer. Experimental results showed that as the moisture content increased, the charge of the granules decreased. The high moisture content affects the permittivity of the object and increases the surface conductivity. This phenomenon stems from the molecular structure of water, because the hydrated ion clusters and their polymers cause the charge dissipation [16]. For moisture content measurement through electrostatic sensing, there is a need to investigate the relationship between the moisture content and the characteristics of the sensor signals.

Preliminary research on the performance of triboelectric probes has been conducted to determine the relationship between the moisture content and the triboelectric signal [17, 18]. Portooghese *et al*. [17] deployed several triboelectric probes at different locations throughout a fluidised bed for real-time measurement of moisture content. The results showed that triboelectric signals were sensitive to the moisture content below 100 ppm [17]. Nonetheless the triboelectric probes need to be installed inside the fluidised bed and it will disturb the movement of the particles. In addition, this method analyses the moisture in a pointwise manner and cannot provide the information about the global moisture content distribution. In

recent years, electrostatic sensor arrays with multiple electrodes have been successfully deployed in a number of applications [19-21]. Zhang *et al*. [21] used a non-intrusive electrostatic sensor array with four sets of electrodes to measure the moisture content of solid particles in a fluidised bed dryer and established a model for the moisture content and the root-mean-square (RMS) magnitude of the electrostatic signal. However, there are only 12 electrodes and the moisture content distribution in the bed cannot be obtained. Moreover, due to the limits of the circuit design, the proposed system has a minimum limit for the moisture content, which is 11 wt.%. Further research is required to develop a new electrostatic sensor array for reconstructing the moisture content distribution in a fluidised bed. Moreover, for gas-solid fluidised beds, it should be emphasized that the presence of bubbles increases the complexity of the moisture content measurement. The mass transfer (i.e. moisture transfer) between the air and the biomass is an important property to understand the drying kinetics, but it is difficult to be predicted analytically [22]. To measure the mass transfer at the gas-solid interface, it is necessary to measure the moisture content distribution and bubble positions.

As indicated in a recent review article by Yan *et al*. [23], there has been little research on the moisture content distribution measurement using electrostatic sensing techniques to date. In this paper, an electrostatic sensor array and an optical digital imaging unit are combined for the first time to measure the moisture content distribution and the moisture transfer at the interface between the air and the biomass. The sensor array is installed on the outer wall of the fluidised bed to sense the moisture content of the biomass. The moisture content distribution is reconstructed using the signals from the multiple electrodes based on a biharmonic spline interpolation (BSI) algorithm. This paper presents the measurement principle, design and implementation of the system. The measurement system is assessed on a laboratory-scale fluidised bed dryer with corn particles under different inlet air velocities and temperatures.

2. Methodology

2.1. Theoretical foundation

In a fluidised bed, triboelectric charging is inevitable as a result of the contact, friction and collision between particle-particle, particle-wall, and particle-air. From the theory of the electrostatic induction, a charged particle and an electrostatic sensor are regarded as an equivalent capacitor, as shown in Fig. 1. The movement of the charged particle with reference to the electrode changes the distance between the two plates of the capacitor and hence the capacitance value [23]. The charge of the particle can be represented by a condenser model as:

$$q=k_c CV = k_c \frac{\varepsilon S}{z} V \tag{1}$$

where q is the charge of the particle, k_c is the charging coefficient, C is the equivalent capacitance and V is the equivalent potential difference. Moreover, ε is the permittivity of the medium, S is the equivalent particle area and z is the distance between a charged particle and an electrode. When the quantity of charges on the particles changes with time, the voltage across the plates also changes. Based on the velocity distribution of the particles in the bed, the radial velocity of the particles is much smaller than the axial velocity [24]. In the measurement system, the sensor is installed on a fixed position, the effect of the distance between the particle

and the electrode on the acquired sensor signal can be neglected since the particles move slowly along the radial direction. Therefore, the signals from the electrostatic sensor can reflect the charge value of the particles.

Fig. 1. Equivalent model of the electrostatic sensor and a charged particle.

The moisture content is an important factor, which leads to the variation of the charge generated on the particles. According to the theory of triboelectrification, a simple model for the dynamics of charging is developed as [25]:

$$\frac{dq}{dt}=\alpha(q_s-q)-\beta q \tag{2}$$

Where q_s is the saturation charge in the absence of leakage, α and β are the charge generation and dissipation coefficients, respectively. In view of the molecular structure of water, a general mechanism of charge dissipation based on hydrated ion clusters $(H_2O)_nH^+$ and $(H_2O)_nOH^-$, and their polymers has been proposed elsewhere [16]. In view of this mechanism, the hydrated ion clusters serve as the main charge carriers to redistribute and dissipate the particles surface charges into free space. The hydrated ions may be naturally formed through a series of reactions, for instance,

$$(H_2O)_n^+ + H_2O \rightarrow OH + (H_2O)_nH^+ \tag{3}$$

$$e^- + (H_2O)_n + OH \rightarrow (H_2O)_nOH^- \tag{4}$$

Because of the mobility of ion clusters and the local electric field in the fluidised bed, numerous agglomerate hydrated ion clusters appear on the wet particle surface, which leads to the very small net charges of particles. In this process, the ion clusters act as the charge carriers when they are in contact with fluidised gas or grounded objects to neutralize (drain off) particle charges, and leave the surrounding environment with space charges (i.e., redistribute the particle charges into space), reducing the amount of charge accumulation [16]. Therefore, information about the moisture content can be obtained by sensing the charged biomass. However, since there is no explicit theoretical equation between the moisture content and charge intensity due to the inherent complexity of the triboelectric charging process. This paper will attempt for the first time to determine the relationship between the key factors through experimental investigations and to accomplish the measurement of the moisture content distribution in a fluidised bed.

2.2. Measurement system

Fig. 2 shows the block diagram of the proposed moisture content distribution measurement system. For measuring the moisture content distribution, an electrostatic sensor array with multiple electrodes is closely attached to the outside wall of the fluidised bed, as shown in Fig. 2. The design of the sensor array and sensitivity distribution of that have been reported in details [26]. When biomass particles are drying in the fluidised bed, they are charged. Hence a certain number of induced charges are generated on the electrode surface with the charged biomass passing through the electrode. The velocity and the moisture content of charged biomass determine the value of the induced charge. The higher velocity and the lower moisture content of the biomass lead to more induced charges on the electrodes and the stronger output signals. From

the information in Fig. 2, the signals from the electrodes are processed using a signal conditioning unit to accomplish the signal conversion, amplification and filtering.

Fig. 2. Block diagram of the moisture content distribution measurement system.

In previous research, the RMS value of the signal from the electrode is often used to represent the magnitude of the signal [21, 23, 27]. Qian *et al*. [27] investigated the effects of moisture content on the electrostatic sensing and measured the RMS values under various moisture content of particles. The results showed that the RMS values reduced with the moisture content. Moreover, the velocity of particle also affects the RMS value as it determines the extent of the triboelectric effect in the fluidised bed. The higher the particle velocity, the more electrostatic charge is generated on particles [28]. For measuring the moisture content using the electrostatic sensing techniques, it is necessary to decouple the effect of the biomass velocity on the RMS value of the electrostatic sensor signal. The biomass velocity (i.e. biomass correlation velocity) is calculated by using the sensor signals with a cross-correlation algorithm [28, 29]. Therefore, with the knowledge of the biomass velocity and the RMS magnitude of the sensor signal, a measurement model for the moisture content is built. The moisture content distribution is reconstructed using the moisture content from multiple electrode pairs based on the BSI algorithm, as illustrated in Fig. 3. An optical digital imaging unit is incorporated to record the positions of bubbles and biomass. The image from a digital camera is cropped to obtain the region of interest (ROI), which has the same size with the image of the reconstructed moisture content distribution. Image processing algorithms are then applied to obtain the bubble distribution. The image is firstly converted into a binary image and segmented using the Otsu's method to distinguish the bubble [26]. Secondly, the pixel coordinates of the bubble boundary in the image are extracted using Canny algorithm [30]. Finally, the moisture content and the mass transfer of the biomass at different positions of the bubble are derived by fusing the information from the moisture content and known positions.

Fig. 3. Information flow of the moisture content distribution measurement system.

2.3. Measurement of biomass velocity

Electrostatic sensors have been successfully used for the velocity measurement of particles in pneumatic conveying pipelines [20]. In comparison with dilute pneumatic conveying pipelines, particle motions in a gas-solid fluidised bed are more complex, which brings challenges to the measurement of particle velocity in the fluidised bed. In the fluidised bed, the sensor signals are measured when charged biomass particles flow through the sensitivity zone of electrostatic sensors. The correlation velocity of the biomass is determined by two signals from upstream and downstream electrodes using the cross-correlation algorithm. As shown in Fig. 4, thirty-two electrodes are divided into twenty-four sets of electrode pairs (namely electrodes A1B1, A2B2, …, B1C1, B2C2, …, C1D1, C2D2, …, C8D8), each set contains two adjacent electrodes in axial direction, which are upstream and downstream electrodes. Every pair of the electrodes (electrodes g and k) are used to measure the particle correlation velocity as

$$v_{gk}(x,y)=\frac{L_{gk}}{\tau_{gk}} \tag{5}$$

Where $v_{gk}(x,y)$ is the particle correlation velocity at centroid position (x,y) of each set of electrode pairs, g, k is A1, A2, …, D8, L_{gk} is the axial distance between electrodes g and k. τ_{gk} is the time delay determined by cross-correlating the signals from upstream and downstream electrodes, which is obtained from locating the dominant peak of the correlation function.

Fig. 4. Schematic diagram of the electrode pairs on the sensor array.

Moreover, it should be stressed that as all the biomass particles in the sensitivity zone of the electrodes contribute to the variation of the sensor signals. The correlation velocity is regarded as the velocity of the particle cloud in the sensitivity zone, which reflects the movement of a number of charged particles. Moreover, the average correlation velocity is always positive due to the larger proportion of the biomass moving upward carried by rising bubbles in the dense phase region [28, 31]. Therefore, the application of cross-correlation calculation to the electrostatic signals could provide a feasible way to characterise the motions of biomass particles and hence offer an important parameter for the moisture content measurement in the fluidised bed dryer.

2.4. Measurement of moisture content distribution

In order to measure the moisture content distribution of the biomass, the relationship between the characteristics of the sensor signal and the moisture content should be determined in advance. Calibration of the measurement system is therefore required in order to derive the moisture content under different operating conditions. In this study, regression analysis is performed to determine the relationship between the characteristics of the sensor signal and the moisture content. The reference moisture content measured using a Halogen Moisture Analyzer, the average RMS magnitude of the sensor signals and the correlation velocities of the particles are analysed to obtain the regression equation. The moisture content during the drying process is determined from

$$M(x,y)=M_0-a\overline{RMS}(x,y)^b \tag{6}$$

where $M(x,y)$ is the moisture content of biomass at position (x,y) of the fluidised bed, M_0 is the initial moisture content, a and b are coefficients which are determined empirically. $\overline{RMS}(x,y)$ is the average RMS magnitude of the two signals on each set of electrode pairs. The coefficient a is related to the particle velocity and is formulated as [21]

$$a=cv_{gk}^{d}+e \tag{7}$$

where c, d and e are coefficients and also determined empirically. In the regression analysis, the velocity (v_{gk}) used in equation (7) is derived by calculating the average correlation velocities from the all sets of the electrode pairs (i.e. twenty-four sets in Fig. 4). Meanwhile, the average RMS ($\overline{RMS}$) used in equation (6) is the arithmetic mean of the RMS values of the signals from all electrodes of the sensor array. For the measurement of the moisture content distribution in the fluidised bed, the signals from each set of the

electrode pairs are employed. From the moisture content measurement model in equation (6), the moisture content of biomass at position (x,y) is obtained. The BSI algorithm is then used to reconstruct the moisture content distribution in the fluidised bed [26]. The image reconstruction is performed on a laptop PC with a 1 GHz Intel Core processor and 8 GB RAM. The BSI algorithm is developed in-house using MATLAB 2017. With this system it takes approximately 0.6 s to reconstruct one image.

3. Experimental setup

In order to assess the performance of the measurement system and investigate the drying kinematic, a series of experiments are conducted on a laboratory-scale test rig. As shown in Fig. 5, the test rig consists of an air compressor, a gas tank, an air preheater and a two dimensional (2D) fluidised bed. The fluidised bed is made of Plexiglas, which has a width of 150 mm, a height of 850 mm, and a thickness of 30 mm. The flow rate of the air is controlled with a needle valve and is measured with a rotameter (relative error is within ±1.5%) during the drying process. A T-type thermocouple with a relative error within ±0.75% was placed at the inlet of the fluidised bed to measure the air temperature. The air temperature was varied between 45 °C and 75°C using a PID-adjusted temperature controller and the air preheater. The electrostatic sensor array was tightly installed on the outside of the fluidised bed wall. The bed wall has a relative permittivity of 3 and a thickness of 10 mm. Both the permittivity of the wall material and the thickness of the wall influence the capacitance between the charged biomass and the electrodes, and hence the sensor signals. In industrial applications, the inner surface of the sensor array should be mounted flush with the inner wall of the fluidised bed, and the electrodes should be insulated from the bed wall. Furthermore, the electrode surface should be covered with a wear-resistant insulating layer to prevent the particle wearing. The electrostatic sensor array was installed in the middle of the dense phase area, which is 100 mm above the distributor. In order to obtain the reference moisture content, samples of approximately 1.5 g at an interval of 5 minutes were taken from the sampling port (100 mm above the distributor), as shown in Fig. 5. The sampled corn particles were collected in a sealed glass bottle. A Halogen Moisture Analyzer (Model HE83, METTLER TOLEDO) was used to measure the reference moisture content of the samples to validate the results from the electrostatic sensor array. When the particles were sampled, the signals from the electrostatic sensor array were recorded simultaneously for 20 s. The signals were acquired using a multiple-channel signal conditioning unit and a NI USB-6363 DAQ with a sampling frequency of 1 kHz [26]. In addition, an imaging system (Fastcam Mini UX50) with 1280 (H) × 1024 (V) pixels was applied to capture the images of the fluid flow in the fluidized bed at a frame rate of 500 fps. The images were used to measure the distribution of the bubbles and biomass. Moreover, a high-intensity uniform illumination system was arranged around the bed whilst a black paper was attached at the back of the fluidized bed in order to ensure good contrast.

Fig. 5. Schematic of the test rig and system installation.

Corn particles with a diameter of 1 mm and a true density of 1100 kg/m^3 are used in the experiments, which are regarded as Geldart D particles. A batch of 1.5 kg wet corn particles with moisture content of around 16.5 wt.% are prepared in advance. Afterwards, the wet particles are kept in a constant temperature humidity

chamber for at least 6 hours to ensure uniform moisture distribution. Before the start of the experiments the wet particles are added to the bed, forming the initial bed height of 200 mm. During the experiments, the relative humidity of the inlet air is constant at 10%. The corn particles are dried under different inlet air velocities and temperatures, which are summarized in Table 1. The minimum fluidisation velocity required to the corn particles is approximately 0.216 m/s.

Table 1 Operating conditions

4. Results and discussion

4.1 Measurement of moisture content

In order to measure the moisture content using the electrostatic sensor array, regression analysis of the average RMS of the signals from the electrodes on the sensor array and the corresponding moisture content is performed. Since the initial moisture content is known for different operating conditions, equation (6) are simplified as

$$\Delta M = a \times \overline{RMS}^{b} \tag{8}$$

Where $\overline{RMS}$ is the average RMS of the total electrodes in the sensor array. From the experimental data under the air velocity of 0.43 m/s with two different temperatures 45ºC and 75ºC (i.e. T1V2 and T3V2), the fitting of equation (8) is shown in Fig. 6. The sensor signals are divided into fourteen segments, and then the average magnitude of each data segment is determined. The average of the fourteen individual magnitude values for the sensor array corresponds to the abscissa of each data point in Fig. 6. The average of the fourteen difference in moisture content measurements corresponds to the ordinate of each data point in Fig. 6. The standard deviation of each data point in Fig. 6 is given as error bars. It can be observed that the average RMS value of the sensor signal increases with the difference in moisture content. The coefficient of determination (R^2) for the fit is 0.93. In addition, the coefficient *a* is related to the biomass correlation velocity and the coefficient *b* is 0.6158, which is determined by averaging the coefficients, as shown in Table 2.

Fig. 6. Regression curve between the RMS magnitude of the sensor signal and the difference in moisture content.

Table 2 Coefficients of *a* and *b*

A power exponent fitted curve of the coefficient *a* and the correlation velocity of the particles is shown in Fig. 7. The R^2 for the fit is 0.99. It is worth noting that the coefficients in equation (6) and (7) need to be determined through the experimental calibration for different biomass and drying processes. The above coefficients are all determined using the least square method. The specific form of equation (6) derived from the fitted curves in Fig. 6 and 7 is as follows

$$M(x,y) = M_0 - \left(0.00253 v_{gk}^{-7.017} + 31.86\right) \overline{RMS}(x,y)^{0.6158} \quad (9)$$

Fig. 7. Regression curve between the correlation velocity of biomass particles and the coefficient *a*.

4.2 Measurement of average moisture content

After the signals from each set of electrode pairs are measured, the moisture content of the biomass in the centroid of each electrode pairs can be determined according to equation (9). The average moisture content in the measurement area is then obtained using the moisture content measurements from twenty-four sets of electrode pairs. Fig. 8 shows the typical average moisture content in the fluidised bed obtained respectively using the electrostatic sensor array and the Halogen Moisture Analyzer under different inlet air velocities. It is obvious that the average moisture content of particles decreases with the drying time. Moreover, the results of the moisture content from the electrostatic sensor array are very close to those from the Halogen Moisture Analyzer (i.e. reference moisture content) under the operating condition of the T2V2. The results from two methods under the operating condition of T2V1 or T2V3 have similar tendencies, but the values of the moisture content have some discrepancies, especially for the later period of the drying. In Fig. 8 (a) the moisture content measured through electrostatic sensing are higher than the reference moisture content. This is because that the lower air velocity decreases the drying efficiency and results in the higher moisture content of the particles, which leads to the smaller amplitude of the sensor signal and the larger measurement error. However, the results are quite different in Fig. 8 (c), the moisture measurements through electrostatic sensing are lower than the reference moisture content. The reason is that with the increase of the air velocity, the flow in the fluidised bed becomes more turbulent and the biomass particles from the sampling port cannot represent the actual moisture content in the whole measurement area.

(a) T2V1 (b) T2V2 (c) T2V3

Fig. 8. Measurement of the average moisture content for different inlet air velocities.

To evaluate the proposed method of the moisture content measurement using the electrostatic sensor array, relative errors between the reference and measured moisture content under different operating conditions are calculated, as shown in Fig. 9. Through the analysis of the measurement results, the relative error for the T2V2 condition is within $\pm 9\%$, which is remarkably more accurate than those for other test condition. This probably due to the fact that the condition of the drying operation (T2V2) is more stable and the moisture content variance of the biomass has little effect on the sensor signals. In addition, it is clear that the relative errors are within $\pm 15\%$ in all cases. The above results demonstrate that the electrostatic sensing is capable of measuring the average moisture content in the fluidised bed with a reasonably accuracy. It should be noted that there are two main sources of measurement error. The first is the systematic error which is caused by the measurement setup. During the calibration, the particles collected from the sampling port are localized particles, which are not exactly the same as the particles in the measurement area detected using the electrostatic sensor array. Moreover, the charge in the fluidised bed is also affected by particle size. The

particle attrition is inevitable during the drying process, leading to measurement errors. Therefore, new sampling devices and modified measurement model which considers the particle size effect should be used to improve the accuracy of the measurement system in future.

Fig. 9. Comparison between the measured and reference moisture contents under different operating conditions.

4.3 Reconstruction of moisture content distribution

The moisture distribution is essential in characterising the spatial behaviour of the bed during drying. The measurement principles in Section 2 show that the electrostatic sensor array has a potential to measure the moisture content distribution in the fluidised bed. The average moisture content and the moisture content distribution are obtained using the signals from each set of the electrode pairs and the regression equation (9), as illustrated in Fig. 10. The picture in the left shows the average moisture content with respect to drying time in the fluidised bed, the pictures in the right show the 2D moisture content distribution with respect to the drying time (the time axis is drawn from bottom to top).

Fig. 10. Average moisture content and the reconstruction of the moisture content distribution (T2V2).

The results show that the biomass moisture content drops from around 16 wt.% to 6 wt.% during the drying period under the operating condition of T2V2. The 2D distribution of the moisture content varies with the drying time. It is worth pointing out that the moisture content distribution also resembles the solids distribution. From the values of the moisture content distribution, the area with small moisture content is regarded as voids or bubbles, while the area with high moisture content is considered as biomass particles [11]. To give a clear presentation of the moisture content distribution as a function of the drying time, the results for three periods (Period I, Period II, Period III) from a single test under the operation condition of T2V2 are presented. Fig. 11 shows the average moisture content and the 2D moisture content distribution at each period.

(a) Period I.

(b) Period II.

(c) Period III.

Fig. 11. Typical results of the average moisture content and the moisture content distribution (T2V2).

With the proposed measurement method, the instantaneous moisture content distribution is obtained, which reflects the fluidisation and operation status of the fluidised bed dryer. Fig. 11 reveals that the biomass particles in the bed are mixed relatively well at the later period (Period III) of the drying, while the bed is almost stagnant at the earlier period (Period I) of the drying. As shown in Fig. 11 (a), the average moisture content of the biomass is almost constant at around 14 wt.% during the Period I. The reason is that the wet

corn particles form agglomerations and sink to the bottom of the fluidised bed at the beginning of the drying due to the high moisture content [32]. The heat and mass transfer rate are low because there is less effective contact between the air and biomass at this period. As the biomass particles are dried, the hydrodynamics of bed changes. Fig. 11 (b) suggests that during the middle drying period (Period II), there are more voids or bubbles in the bed and the average moisture content curve displays a clear fluctuation (12 wt.%-13 wt.%). This is because as the biomass particles are dried, the moisture content of the biomass gets lower which prevents them from agglomeration and the air drives biomass to the top of the bed with the aid of the drag force, facilitating the particles mixing. Fig. 11 (c) shows the average moisture content fluctuates from 5.6 wt.% to 8.9 wt.% in the later drying period (Period III) and the drying curve shows a more unstable trend than the former drying periods. In the later drying period, the flow in the fluidised bed becomes more turbulent, which leads to the unstable drying operation.

4.4 Comparison of results from electrostatic sensing and digital imaging

For gas-solid fluidised beds, it should be emphasized that bubbles formed at the distributor move upwards and act on the biomass particles, where convective mass transfer also occurs [4, 22]. However, the presence of bubbles increases the complexity of the drying kinetics in the fluidised bed. The moisture content distribution and the bubble distribution are determined using the results from the electrostatic sensor array and the digital imaging, respectively. From the above results, the mass transfer between the air and the biomass at different positions of the bubble can be fully explored. As shown in Fig. 12, the moisture content distribution measured from the electrostatic sensor array is compared with the images from the digital camera.

(a) Images from the digital camera.

(b) Moisture content distribution reconstructed from the electrostatic sensing system.

(c) Fusion image.

Fig. 12. Comparison of the results from the electrostatic sensing and digital imaging systems.

In the experiments, results from the electrostatic sensor array and the digital camera are measured simultaneously. The image from the digital camera is cropped to obtain the ROI with a total of 379 (H) × 142 (V) pixels. The image processing algorithms are then applied to obtain the bubble distribution in Fig. 12 (a). Using the proposed method, the moisture content distribution at the same time is reconstructed, as shown in Fig. 12 (b). Then the position of the bubble boundary is marked in the reconstructed the moisture content distribution, forming a fusion image (Fig. 12 (c)). Finally, the moisture contents at positions of the bubble boundary, bubble interior and bubble exterior are obtained from the moisture content distribution in corresponding pixels, respectively. The moisture content of biomass at different positions during a typical drying process is shown in Fig. 13.

Fig. 13. Moisture content distribution of biomass at different positions.

The fusion images in Fig.13 show a typical process of bubbles generating, contacting and coalescing. At 2071 s, the biomass particles inside the two bubbles are mixed well with the hot air. The convective mass transfer occurs and the moisture content of the biomass in the bubble interior and boundary is low. However, biomass particles in the bubble exterior have a higher moisture content, because they are far from the bubbles. The two bubbles contact each other at 2072 s and the biomass particles in the bubble boundary have lower moisture content than that in the bubble interior. Especially biomass particles at the positions of the right boundary of the left bubble and the left boundary of the right bubble are much more dryer because the particles contact with both bubbles with a higher mass transfer rate. When it comes to the results at 2073 s, the two bubbles coalesce into a big bubble. The moisture content of particles in the bubble boundary and interior is lower than that in the bubble exterior. There is stable mass transfer at the interface between biomass particles and the bubble because the former have sufficient contact time with the hot air. In summary, the proposed moisture content analysis method, which fuses the results from the electrostatic sensor array and the digital imaging, has revealed the mass transfer characteristics in the fluidised bed dryer.

5. Conclusions

A novel measurement system using an electrostatic sensor array and an optical digital imaging unit has been designed and implemented to measure the moisture content distribution of biomass in the fluidised bed dryer. The signals from the multiple electrodes have been used to measure the correlation velocity of the biomass and a measurement model has been proposed based on the regression analysis of the sensor signal and the moisture content. A series of experimental investigations of the corn particles have been conducted. The experimental results have demonstrated that the electrostatic sensor array is capable of measuring the moisture content and the relative error is no greater than ±15% over the inlet air velocity from 0.37 m/s to 0.49 m/s and temperature from 45ºC to 75ºC. In addition, the 2D distributions of the moisture content in the dryer have been reconstructed during the three typical periods of the drying process. The results reveal that the bed is mixed relatively well at the later period of the drying with better mass transfer between the biomass and bubbles, while the bed is almost stagnant at the earlier period of the drying due to the high moisture content. By fusing the results from the electrostatic sensor array and the optical digital imaging unit, the mass transfer between the air and the biomass at different positions of the bubble have been compared. The results have shown that when the two bubbles coalesce, the moisture content of biomass in the bubble boundary is higher than that at other positions because of the stable mass transfer at the interface. Moreover, with further development in the sensor design and reconstruction algorithms, the proposed method will be deployed on a 3D fluidised bed in the near future.

Acknowledgement

This work is supported by the National Natural Science Foundation of China (No. 61403138) and Beijing Natural Science Foundation (No. 3202028).

References

[1] W.B. Zhang, X.F. Cheng, Y.H. Hu, Y. Yan, Online prediction of biomass moisture content in a fluidised bed dryer using electrostatic sensor arrays and the Random Forest method, Fuel 239 (2019) 437–445.

[2] M. Aghbashlo, R. Sotudeh-Gharebagh, R. Zarghami, A.S. Mujumdar, N. Mostoufi, Measurement techniques to monitor and control fluidization quality in fluidised bed dryers: a review, Dry Technol. 32 (2014) 1005–1051.

[3] H.J. Das, P. Mahanta, R. Saikia, M.S. Aamir, Performance evaluation of drying characteristics in conical bubbling fluidized bed dryer, Powder Technol. 374 (2020) 534-543.

[4] D. Jia, X.T. Bi, C. J. Lim, S. Sokhansanj, Atsushi Tsutsumi, Gas-solid mixing and mass transfer in a tapered fluidized bed of biomass with pulsed gas flow, Powder Technol. 316 (2017) 373–387.

[5] R. Sivakumar, R. Saravanan, A. Elaya Perumal, S. Iniyan, Fluidised bed drying of some agro products – A review, Renew. Sust. Energ. Rev. 61 (2016) 280–301.

[6] H.J. He, D. Wu, D.W. Sun, Non-destructive and rapid analysis of moisture distribution in farmed Atlantic salmon (Salmo salar) fillets using visible and near-infrared hyperspectral imaging, Innov. Food Sci. Emerg. 18 (2013) 237–245.

[7] J. Sun, X. Zhou, Y.G. Hu, X.H. Wu, X.D. Zhang, P. Wang, Visualizing distribution of moisture content in tea leaves using optimization algorithms and NIR hyperspectral imaging, Comput. Electron. Agr. 160 (2019) 153–159.

[8] A.K. Horigane, K. Suzuki, M. Yoshida, Moisture distribution in rice grains used for sake brewing analyzed by magnetic resonance imaging, J. Cereal Sci. 60 (2014) 193-201.

[9] K. Watanabe, C. Lazarescu, S. Shida, S. Avramidis, A novel method of measuring moisture content distribution in timber during drying using CT scanning and image processing techniques, Dry. Technol. 30 (2012) 256–262.

[10] H.G. Wang, W.Q. Yang, P. Senior, R.S. Raghavan, S.R. Duncan, Investigation of batch fluidized-bed drying by mathematical modeling, CFD simulation and ECT measurement, AICHE J. 54 (2008) 427–444.

[11] V. Rimpilainen, L.M. Heikkinen, M. Vauhkonen, Moisture distribution and hydrodynamics of wet granules during fluidised-bed drying characterized with volumetric electrical capacitance tomography, Chem. Eng. Sci. 75 (2012) 220–234.

[12] T. Antequera, D. Caballeroa, S. Grassi, B. Uttaro, T. Perez-Palaciosa, Evaluation of fresh meat quality by Hyperspectral Imaging (HSI), Nuclear Magnetic Resonance (NMR) and Magnetic Resonance Imaging (MRI): A review, Meat Sci. 172 (2021) 108340.

[13] F. Fotovat, X.T. Bi, J.R. Grace, A perspective on electrostatics in gas-solid fluidised beds: Challenges and future research needs, Powder Technol. 329 (2018) 65–75.

[14] K. Choi, M. Taghavivand, L.F. Zhang, Experimental studies on the effect of moisture content and volume resistivity on electrostatic behaviour of pharmaceutical powders, Int. J. Pharmaceut. 519 (2017) 98–103.

[15] M. Taghavivand, K. Choi, L.F. Zhang, Investigation on drying kinetics and tribocharging behaviour of pharmaceutical granules in a fluidised bed dryer, Powder Technol. 316 (2017) 171–180.

[16] T. Nguyen, S. Nieh, The role of water vapour in the charge elimination process for flowing powders, J. Electrostat. 22 (1989) 213-227.

[17] F. Portoghese, F. Berruti, C. Briens, Continuous on-line measurement of solid moisture content during fluidised bed drying using triboelectric probes, Powder Technol. 181 (2008) 169–177.

[18] Y. Li, M. Jahanmiri, F.S. Careaga, C. Briens, F. Berruti, J. McMillan, Applications of electrostatic probes in fluidized beds, Powder Technol. 370 (2020) 64–79.

[19] H. Zhou, Y. Yang, K. Dong, J. Wu, Y. Yan, X. Qian, K. Cen, Investigation of two-phase flow mixing mechanism of a swirl burner using an electrostatic sensor array system, Flow Meas. Instrum. 32 (2013) 14–26.

[20] X.C. Qian, Y. Yan, S.T. Wu, S. Zhang, Measurement of velocity and concentration profiles of pneumatically conveyed particles in a square-shaped pipe using electrostatic sensor arrays, Powder Technol. 377 (2021) 693–708.

[21] W.B. Zhang, X.F. Cheng, Y.H. Hu, Y. Yan, Measurement of moisture content in a fluidised bed dryer using an electrostatic sensor array, Powder Technol. 325 (2018) 49–57.

[22] R.M. Moreno, G. Antolin, A.E. Reyes, Mass transfer during forest biomass particles drying in a fluidised bed, Biosyst. Eng. 198 (2020)163–171.

[23] Y. Yan, Y.H. Hu, L.J. Wang, X.C. Qian, W.B. Zhang, K. Reda, J.L. Wu, G. Zheng, Electrostatic sensors – Their principles and applications, Measurement 169 (2021) 108506.

[24] T.Y. Wang, T.Q. Tang, Q.H. Gao, Z.G. Yuan, Y.R. He, Experimental and numerical investigations on the particle behaviours in a bubbling fluidized bed with binary solids, Powder Technol. 362 (2020) 436–449.

[25] W.D. Greason, Investigation of a test methodology for triboelectrfication, J. Electrostat. 49 (2000) 245-256.

[26] B.J. Qi, W.B. Zhang, Y. Yan, X.Y. Li, Experimental investigations into bubble characteristics in a fluidized bed through electrostatic imaging, IEEE Trans. Instrum. Meas. 70 (2021) 9503813.

[27] X.C. Qian, D.P. Shi, Y. Yan, W.B. Zhang, G.G. Li, Effects of moisture content on electrostatic sensing based mass flow measurement of pneumatically conveyed particles, Powder Technol. 311 (2017) 579–588.

[28] Y. Yang, Q. Zhang, C. Zi, Z.L. Huang, W.B. Zhang, Z.W. Liao, J.D. Wang, Y.R. Yang, Y. Yan, G.D. Han, Monitoring of particle motions in gas-solid fluidised beds by electrostatic sensors, Powder Technol. 308(2017) 461–471.

[29] W.B. Zhang, Y. Yan, Y. Yang, J.D. Wang, Measurement of flow characteristics in a bubbling fluidised bed using electrostatic sensor arrays, IEEE Trans. Instrum. Meas. 65 (2016) 703-712.

[30] T.R. Fujimoto, T. Kawasaki, K. Kitamura, Canny-Edge-Detection/Rankine-Hugoniot-conditions unified shock sensor for inviscid and viscous flows, J. Comput. Phys. 396 (2019) 264–279.

[31] W.B. Zhang, T.Y. Wang, Y.Y. Liu, W.B. Zhan, C.H. Wang, Particle velocity measurement of binary mixtures in the riser of a circulating fluidised bed by the combined use of electrostatic sensing and high-speed imaging, Petrol. Sci. 17 (2020) 1159–1170.

[32] M. Farkhondehkavaki, M. Soleimani, M. Latifi, F. Berruti, C. Briens, J. McMillan, Characterization of moisture distribution in a fluidized bed, Measurement 47 (2014) 150–160.

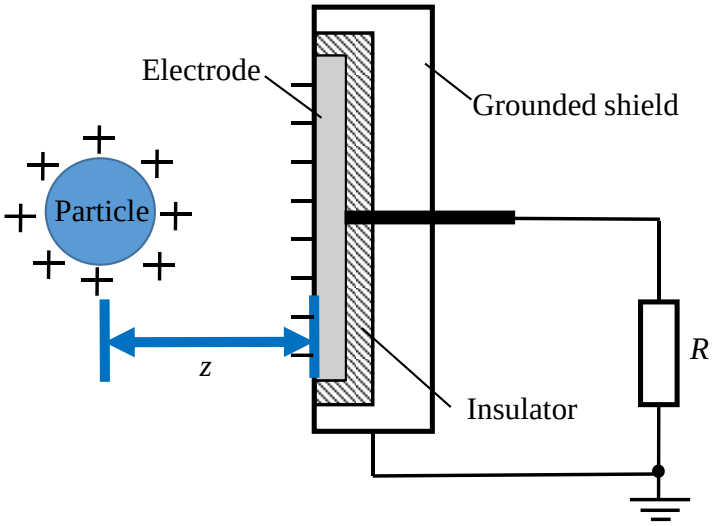

Fig. 1. Equivalent model of the electrostatic sensor and a charged particle.

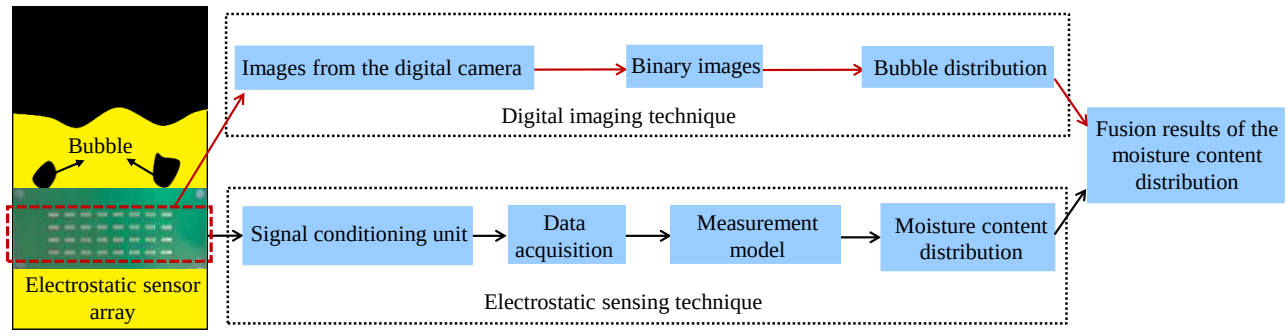

Fig. 2. Block diagram of the moisture content distribution measurement system.

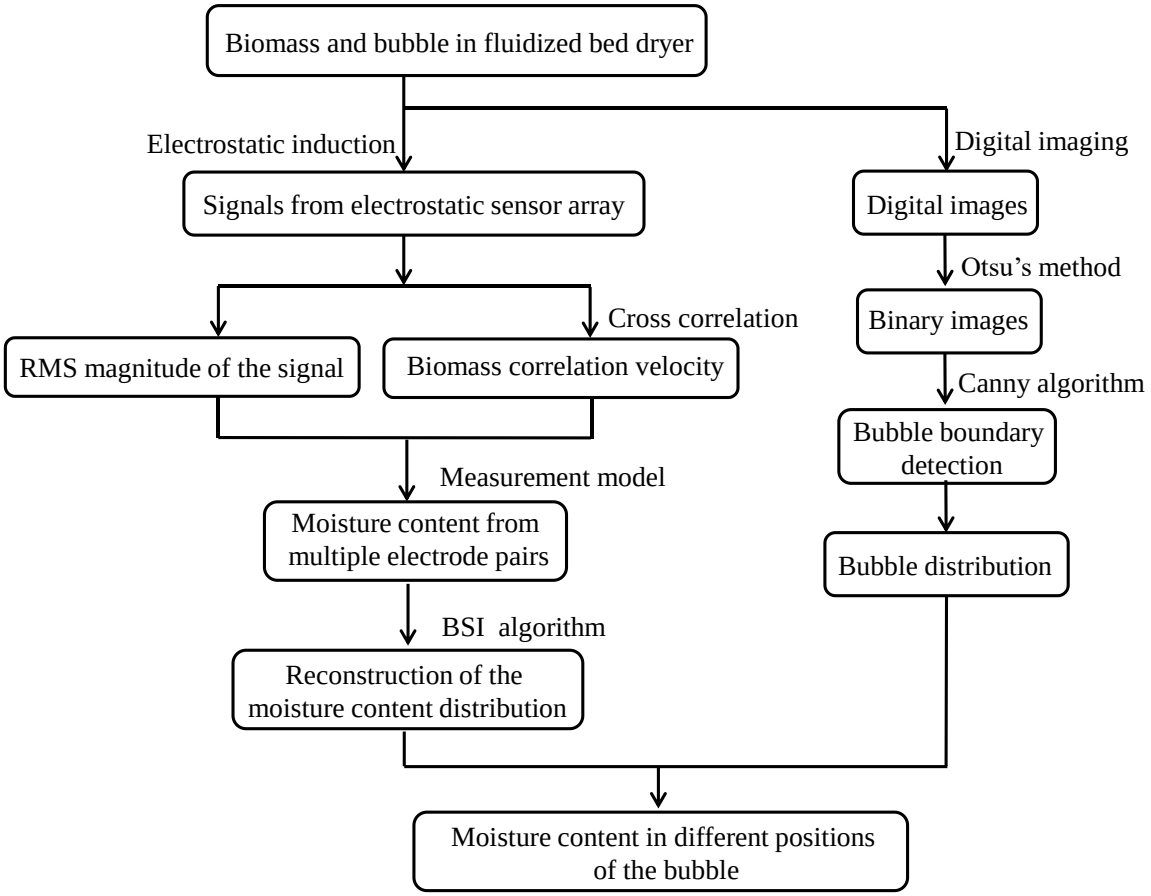

559

560 **Fig. 3.** Information flow of the moisture content distribution measurement system.

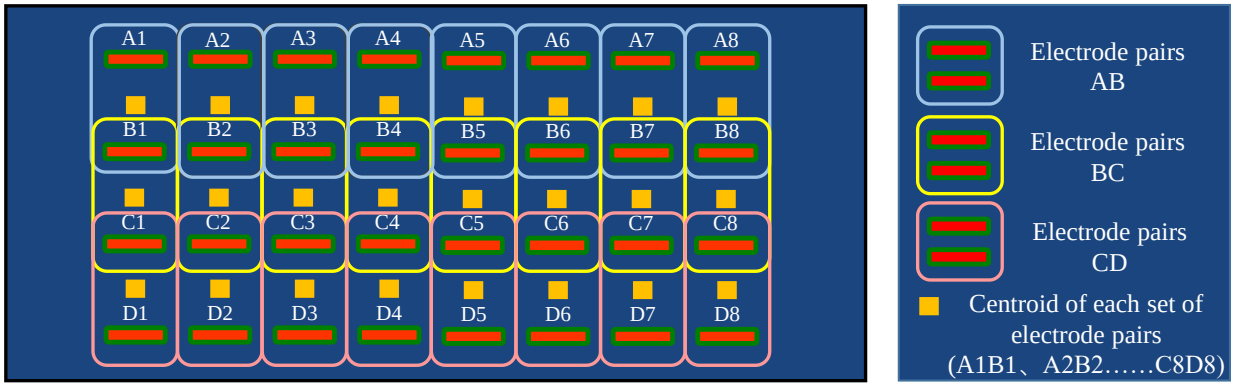

561

562 **Fig. 4.** Schematic diagram of the electrode pairs on the sensor array.

563

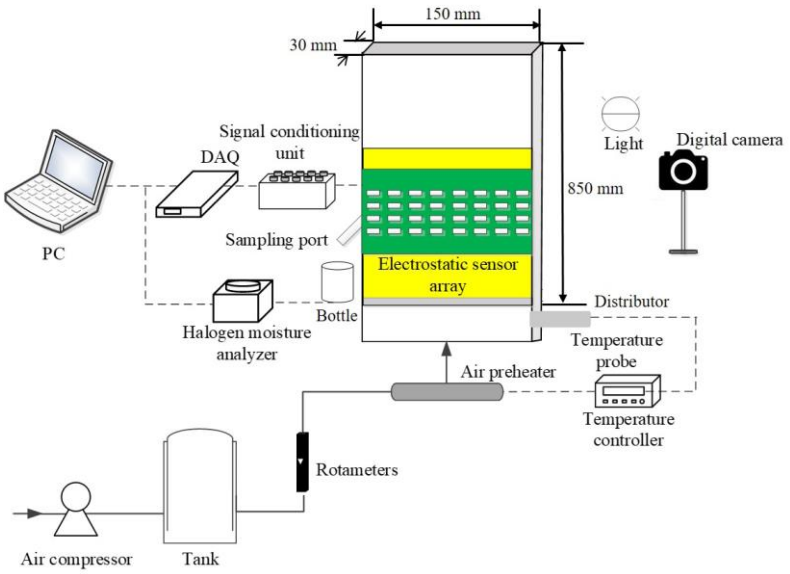

564

565 **Fig. 5.** Schematic of the test rig and system installation.

566

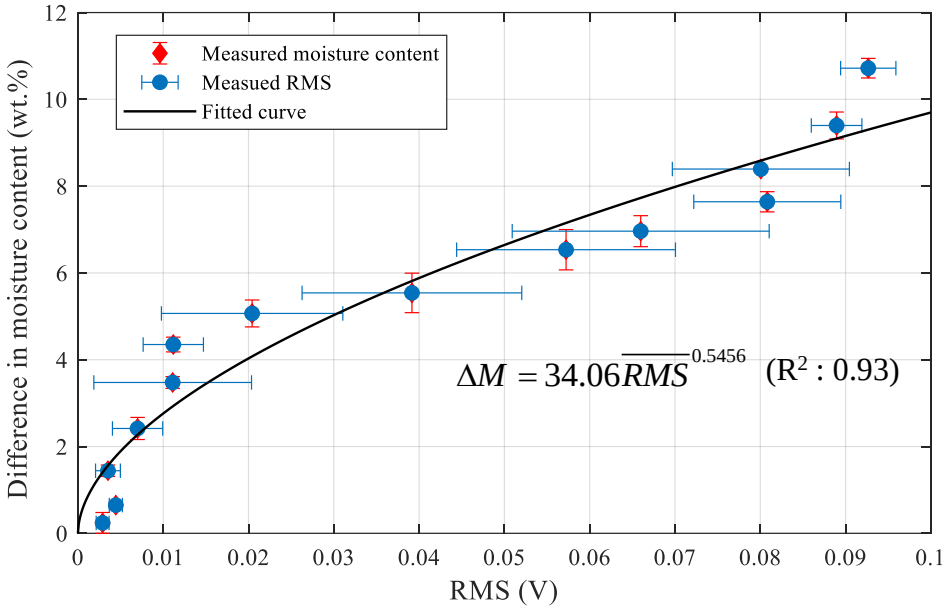

Fig. 6. Regression curve between the RMS magnitude of the sensor signal and the difference in moisture content.

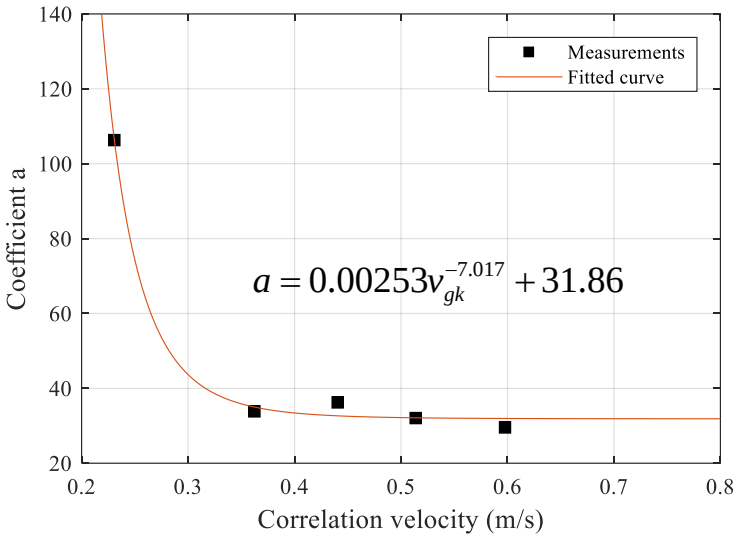

570

571 **Fig. 7.** Regression curve between the correlation velocity of biomass particles and the coefficient *a*.

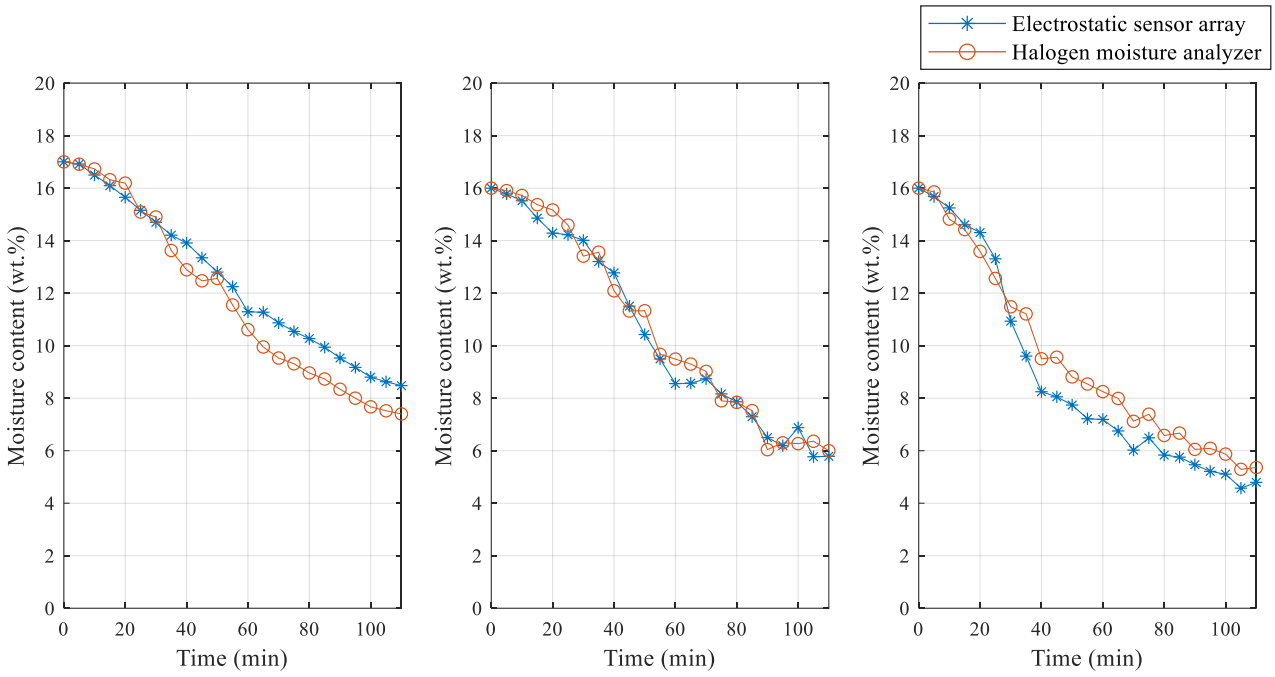

572

573 (a) T2V1 (b) T2V2 (c) T2V3

574 **Fig. 8.** Measurement of the average moisture content for different inlet air velocities.

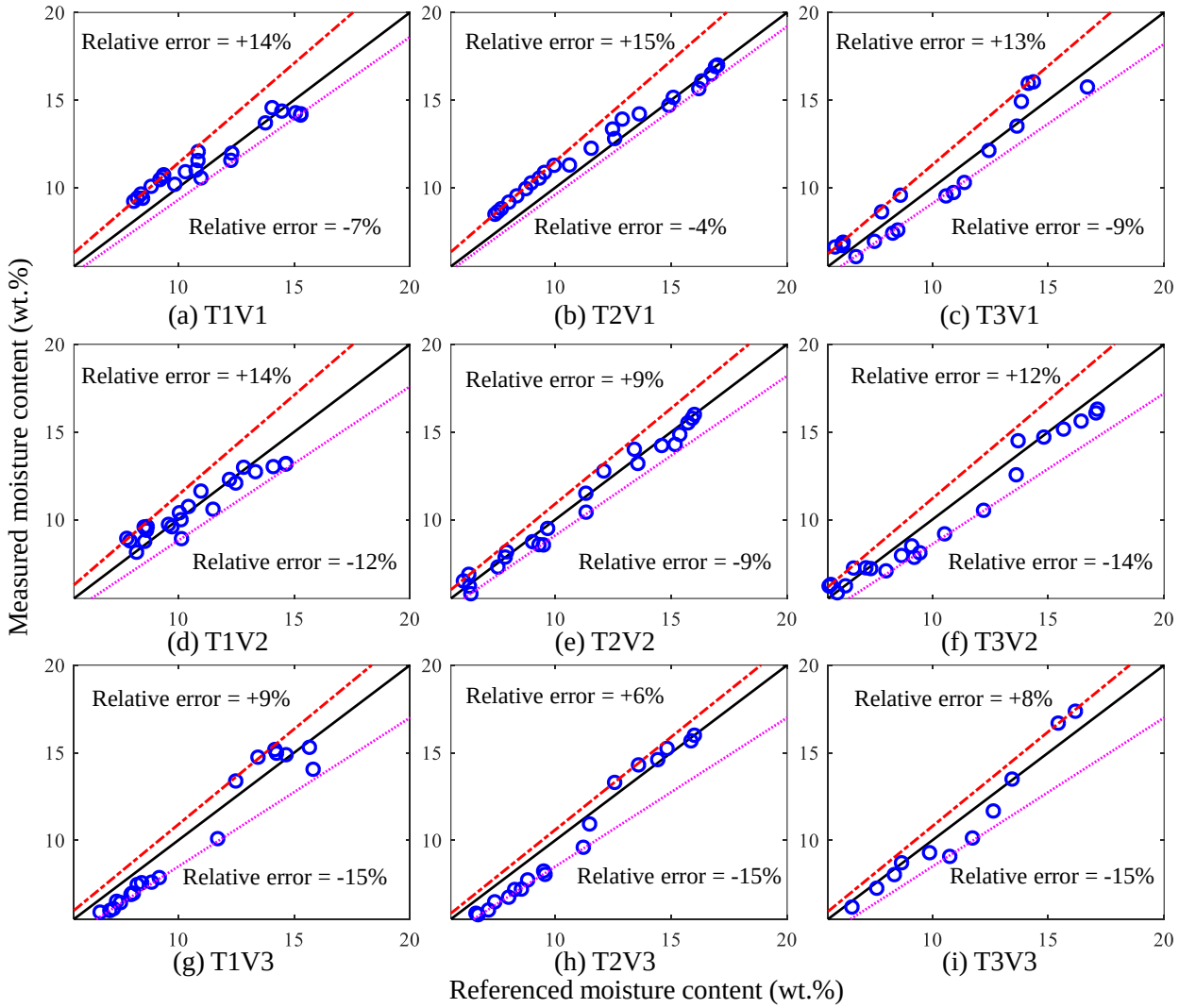

575

576 **Fig. 9.** Comparison between the measured and reference moisture contents under different operating
577 conditions.

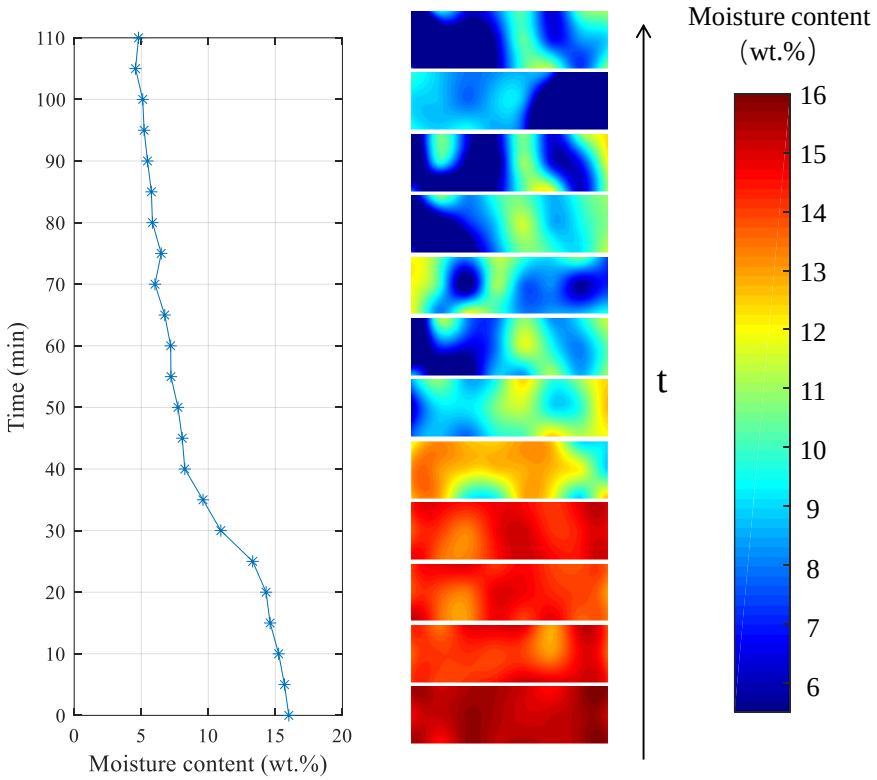

Fig. 10. Average moisture content and the reconstruction of the moisture content distribution (T2V2).

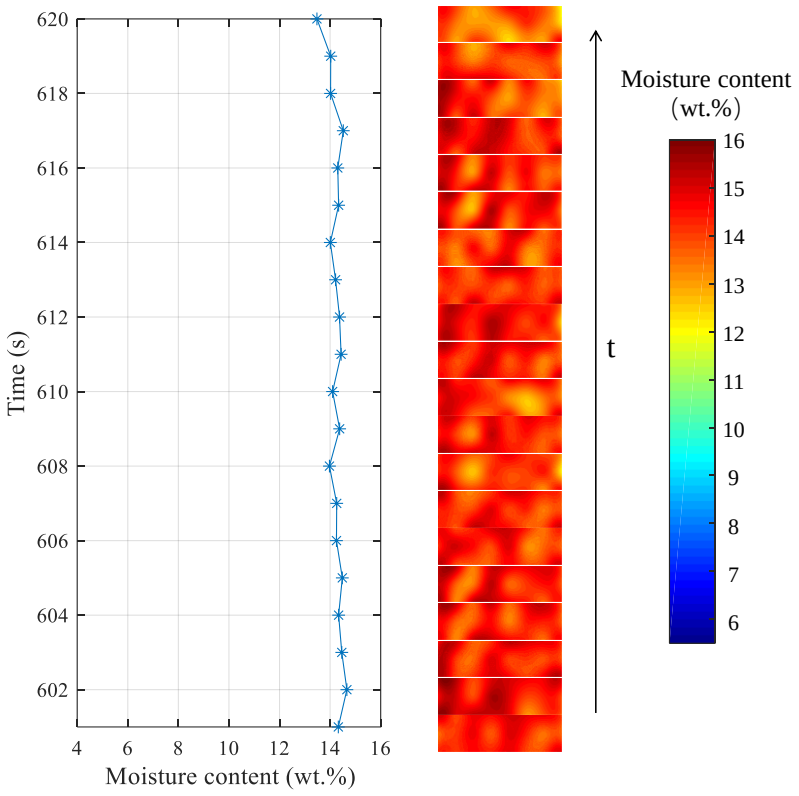

580

581 (a) Period I.

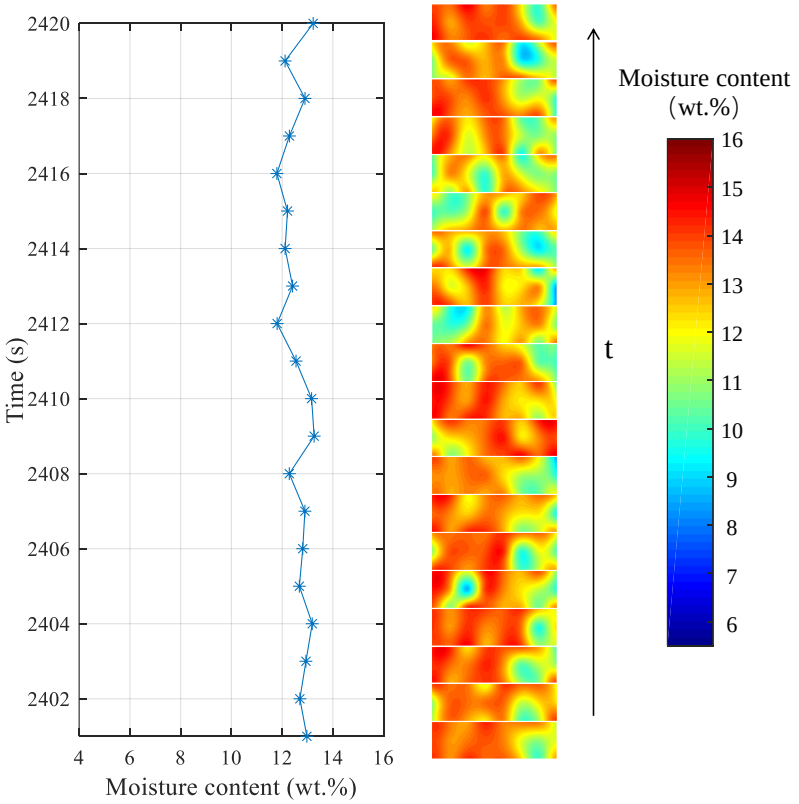

582

583 (b) Period II.

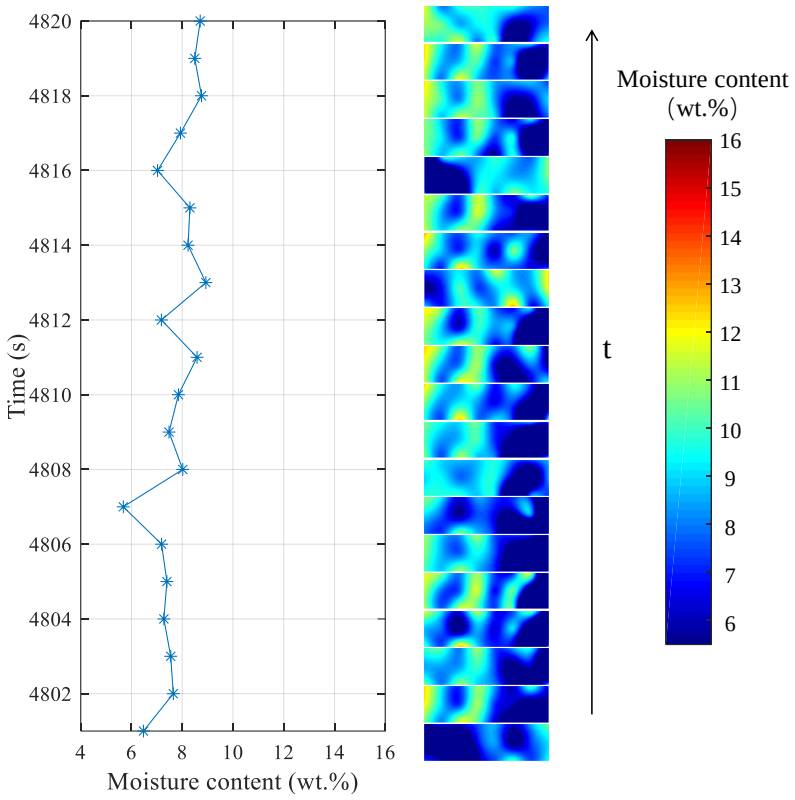

(c) Period III.

Fig. 11. Typical results of the average moisture content and the moisture content distribution (T2V2).

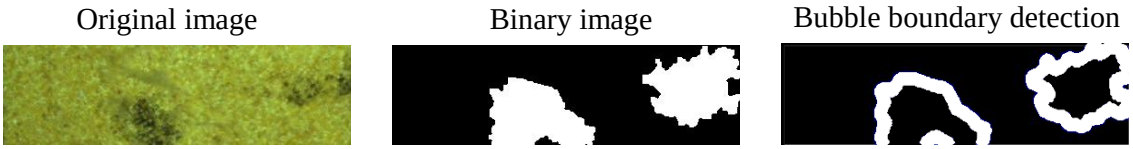

(a) Images from the digital camera.

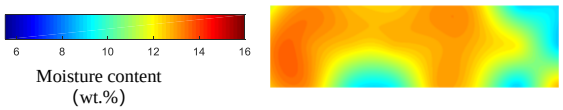

(b) Moisture content distribution reconstructed from the electrostatic sensing system.

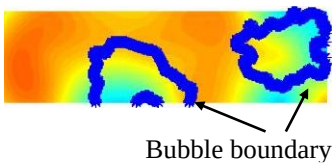

(c) Fusion image.

Fig. 12. Comparison of the results from the electrostatic sensing and digital imaging systems.

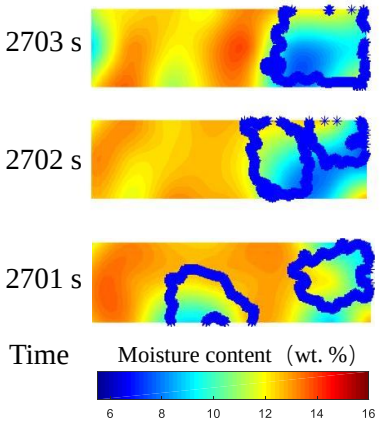

596

597 **Fig. 13.** Moisture content distribution of biomass at different positions.

598

599 **Table 1** Operating conditions

Air velocity (m/s)	Temperature (℃)		
	45	**60**	**75**
0.37	T1V1	T2V1	T3V1
0.43	T1V2	T2V2	T3V2
0.49	T1V3	T2V3	T3V3

600

601 **Table 2** Coefficients of *a* and *b*

602

Correlation velocity (m/s)	***a***	***b***
0.23	106.30	0.6830
0.36	33.85	0.5498
0.44	41.24	0.6878
0.51	32.06	0.5717
0.60	29.56	0.5869